GOUX, C. (1961). *Mem. Sci. Rev. Metall.* **58**, 661–676.
KRIVY, K. & GRUBER, B. (1976). *Acta Cryst.* A**32**, 297–298.
MACKENZIE, J. K. (1958). *Biometrika*, **45**, 229–240.
MITCHELL, C. M. (1979). Private communication.
RANGANATHAN, S. (1966). *Acta Cryst.* **21**, 197–199.
SANTORO, A. & MIGHELL, A. D. (1973). *Acta Cryst.* A**29**, 169–175.
WARRINGTON, D. H. (1975). *J. Phys.* (*Paris*), **36**, (Suppl. to No. 10), C4-87–C4-95.
WARRINGTON, D. H. & BUFALINI, P. (1971). *Scr. Metall.* **5**, 771–776.

Acta Cryst. (1981). A**37**, 189–196

Application of Cylindrical Distribution Functions to Wide-Angle X-ray Scattering from Oriented Polymers

BY GEOFFREY R. MITCHELL AND RICHARD LOVELL

Department of Metallurgy & Materials Science, University of Cambridge, Pembroke Street, Cambridge CB2 3QZ, England

(*Received* 14 *August* 1980; *accepted* 23 *September* 1980)

Abstract

A systematic approach is presented for obtaining cylindrical distribution functions (CDF's) of non-crystalline polymers which have been oriented by extension. The scattering patterns and CDF's are also sharpened by the method proposed by Deas and by Ruland. Data from atactic poly(methyl methacrylate) and polystyrene are analysed by these techniques. The methods could also be usefully applied to liquid crystals.

1. Introduction

There are two reasons for investigating the wide-angle X-ray scattering (WAXS) from oriented non-crystalline polymers. Firstly, it can aid in the interpretation of features in the scattering [or in the radial distribution function (RDF)] of unoriented polymers, by separating peaks into those from scattering within chains and those from scattering between chains (Lovell, Mitchell & Windle, 1980). Secondly, it may show changes in structure that take place when the polymer is deformed. In this paper we present a systematic approach to the calculation of cylindrical distribution functions (CDF's) which assists both these aims.

To investigate the structure of unoriented polymers, we have previously adopted the technique of comparing scattering calculated for models with that measured experimentally (*i.e.* the comparison is made in reciprocal space). Peaks in the experimental scattering can be separated into intrachain peaks, which intensify towards the extension direction (meridian) when the material is deformed, and interchain peaks, which intensify perpendicular to the extension direction (towards the equator). This separation cannot easily be carried over into the RDF since features in the RDF come from more than one peak in the scattering. Hence a CDF (or at least its meridional and equatorial sections) must be prepared for the deformed materials before the RDF can be reliably separated into intrachain and interchain features.

To investigate the structure of oriented polymers, we have also made the comparisons in reciprocal space by using an azimuthal sharpening technique to improve the apparent degree of chain orientation (Lovell & Windle, 1976, 1977). This gives a pattern similar to a diffuse fibre pattern which may be more easily interpreted. Although unoriented polymers are frequently analysed with RDF's, few workers have prepared CDF's for oriented polymers since Norman (1954) first calculated the CDF of cellulose. This may be due to the difficulty of interpretation since, as we hope to show, CDF's are not much more difficult to prepare than RDF's.

We shall first compare the two methods which have been used for calculating CDF's and show how intermediate results in the procedure can assist in their interpretation. The approach is then illustrated with results from poly(methyl methacrylate) (PMMA) and polystyrene (PS) deformed close to their glass-transition temperatures.

2. Cylindrical distribution functions

The CDF is the cylindrical average of the normalized self-convolution of the electron density, and is defined by

$$W(\mathbf{r}) = 4\pi r[\rho(\mathbf{r}) - \rho_0]$$

0567-7394/81/020189-08$01.00

The formulae relating it to the two-dimensional scattering $i(\mathbf{s})$ depend on the coordinate system used. Fig. 1 illustrates both cylindrical and spherical coordinate systems in reciprocal space.

2.1. *Cylindrical coordinates*

For cylindrical coordinates, the CDF is given by (Wrinch, 1946; Alexander, 1969, p. 461)

$$W(R,Z) = \frac{2r}{\pi} \int_0^\infty \int_0^\infty R' i(R',Z') J_0(RR') \times \cos(ZZ')\, dR'\, dZ' \qquad (1)$$

where J_0 is the zero-order Bessel function,

$$R = |\mathbf{r}| \sin\alpha, \quad Z = |\mathbf{r}| \cos\alpha$$

and $i(R',Z')$ is the reduced scattered intensity.

This expression has the obvious advantages of compactness and of only using one order of Bessel function. However, the double integral results in considerable computation, although this is not a serious drawback with fast computers. Conventional diffraction equipment generally operates with a spherical coordinate system, so the use of (1) would necessitate two-dimensional interpolation.

The principal problem, having obtained reliable fully corrected data, in carrying out any transformation is the limited region of reciprocal space for which experimental data can be collected. We have shown (Lovell, Mitchell & Windle, 1979) that this termination error in a one-dimensional transform can be minimized by calculating the transform at points with a spacing representing the inherent resolution, and positions determined by the form of the reduced intensity at the termination point. The two integrals of (1) produce two termination errors and, although the transform could be calculated at the correct resolution, the large isotropic portion of the scattering will cause the value of the reduced intensity at the termination point to vary considerably and hence make termination error difficult to avoid.

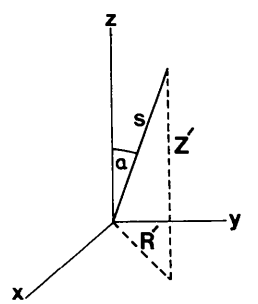

Fig. 1. Cylindrical (R',Z') and spherical (s,α) coordinates in reciprocal space. $s = 4\pi \sin\theta/\lambda$.

2.2. *Spherical coordinates*

In spherical coordinates, any cylindrically symmetric function with an inversion centre, such as $i(s,\alpha)$, can be expanded in a series of Legendre polynomials of even order:

$$i(s,\alpha) = \sum_{n=0}^{\infty} i_{2n}(s) P_{2n}(\cos\alpha), \qquad (2)$$

where

$$i_{2n}(s) = (4n+1) \int_0^{\pi/2} i(s,\alpha) P_{2n}(\cos\alpha) \sin\alpha\, d\alpha \qquad (3)$$

and P_{2n} are Legendre polynomials. This expansion is analogous to Fourier series for linearly periodic functions.

The CDF can also be expanded in such a series:

$$W(r,\alpha) = \sum_{n=0}^{\infty} W_{2n}(r) P_{2n}(\cos\alpha) \qquad (4)$$

and Deas (1952) has shown that the coefficients are related to those of the scattering by

$$W_{2n}(r) = (-1)^n \frac{2r}{\pi} \int_0^\infty s^2 i_{2n}(s) j_{2n}(rs)\, ds, \qquad (5)$$

where j_{2n} are spherical Bessel functions. For small departures from isotropy, only a few terms are needed in the expansion. The first term of (4) will be dominant and this is identical with the RDF for isotropic systems.

The seemingly more involved set of expressions derived for spherical coordinates has considerable advantages. The most immediate is that the data may be collected in this coordinate system. Moreover, only single integrals and a single termination are involved and hence termination errors may be more easily avoided, particularly if (as is usually true) the scattering is isotropic at high s values. The only minor drawback to the method is the use of higher orders of spherical Bessel functions and Legendre polynomials.

We will now consider in more detail the experimental procedure, data correction and numerical methods for the spherical coordinate system.

3. Experimental procedure

The symmetrical transmission geometry together with the incident beam monochromator were the same as used by Pick, Lovell & Windle (1980). The data were collected at intervals of 1° in 2θ (Cu $K\alpha$ radiation) and 9° in α. They were smoothed and interpolated on to an equal-interval grid with $\Delta s = 0{\cdot}1$ Å^{-1} and $\Delta\alpha = \pi/80$ rad. (The value of $\Delta\alpha$ used depends on the degree of anisotropy present, *i.e.* on the highest order of Legendre polynomial needed. An interval of $\pi/80$ is adequate for $2n = 0$ to 12.)

The data were corrected for absorption and polarization (Alexander, 1969, pp. 72, 40), and for multiple scattering. For the latter correction the method of Dwiggins (1972) was used, although for the s range used the correction was very small. From the corrected data $I_{corr}(s,\alpha)$, an azimuthally averaged intensity function may be calculated:

$$I_{av}(s) = \int_0^{\pi/2} I_{corr}(s,\alpha) \sin\alpha \, d\alpha,$$

which is then normalized to the independent scattering [coherent, $\sum f^2(s)$, plus Compton, $I_{Comp}(s)$] from an average atom by the method of Krogh-Moe (1956). The two-dimensional data can now be normalized with the same normalization factor, k, and the independent scattering is then subtracted. This removes the large intraatomic peak near the origin in the CDF.

The reduced intensity is then given by

$$i(s,\alpha) = \frac{kI_{corr}(s,\alpha) - I_{Comp}(s) - \sum f^2(s)}{g^2(s)},$$

where $g^2(s)$ is an arbitrary sharpening function (Warren, 1969). $g^2(s) = 1$ gives an electronic CDF, whereas $g^2(s) = [\sum f(s)]^2$ gives an atomic CDF. There is, however, little difference between the two forms of CDF beyond 3–4 Å, so we have used $g^2(s) = 1$.

A further refinement might be to subtract the scattering from all fixed distances r_{jk} within the chain by replacing $\sum f^2$ with $\sum_j \sum_k (f_j f_k \sin r_{jk}s)/r_{jk}s$ (Waring, Lovell, Mitchell & Windle, 1981). This would show the interchain scattering more distinctly.

The transformation of $i(s,\alpha)$ is performed with (2) to (5). The Legendre polynomials and spherical Bessel functions needed up to $2n = 6$ are given in Table 1. Higher-order Legendre polynomials were obtained from the forward recurrence relation:

$$P_n(x) = \frac{1}{n}[(2n-1)xP_{n-1}(x) - (n-1)P_{n-2}(x)],$$

whereas higher-order spherical Bessel functions were calculated from the backward recurrence relation:

$$j_n(x) = \frac{2n+3}{x} j_{n+1}(x) - j_{n+2}(x)$$

(Abramowitz & Stegun, 1965). For large values of x,

$$j_{2n}(x) \to (-1)^n \frac{1}{x} \sin x$$

and therefore all spherical Bessel functions of even order are in phase at large x. Hence the integral of (5) becomes a Fourier transform for large values of rs:

$$W_{2n}(r) \to \frac{2}{\pi} \int_0^{\infty} si_{2n}(s) \sin rs \, ds$$

and so the termination error for all components may be minimized by the sampled transform technique (Lovell, Mitchell & Windle, 1979). Sampling the transform at the points $(2m + 1)\pi/2s_{max}$ gives an error in W_{2n} proportional to $1/r^2$ times the gradient of i_{2n} at the cut-off point (s_{max}). For PMMA, this gradient is small for i_0 and zero for the higher-order components. Hence the error should be small. For PS, the gradient of i_0 at s_{max} is larger but the anisotropic component has almost zero gradient.

Since (5) is an exact Fourier transform when $n = 0$, Filon's (1929) method was used to calculate W_0 from i_0, whereas the other integrals were calculated by Simpson's rule.

4. Azimuthal sharpening

In our earlier work on oriented polymers, we developed an approximate numerical technique for azimuthally sharpening the scattering patterns (Lovell & Windle, 1977). There is, however, an exact solution in terms of expansions in Legendre polynomials, which was originally suggested by Deas (1952) and rederived by Ruland (1977), but the method has not previously been applied to experimental data.

Table 1. *Legendre polynomials $P_n(x)$ and spherical Bessel functions $j_n(x)$ of even order*

n	$P_n(x)$	$j_n(x)$
0	1	$\frac{\sin x}{x}$
2	$\frac{1}{2}(3x^2 - 1)$	$\left(\frac{3}{x^2} - 1\right)\frac{\sin x}{x} - \frac{3}{x^2}\cos x$
4	$\frac{1}{8}(35x^4 - 30x^2 + 3)$	$\left(\frac{105}{x^4} - \frac{45}{x^2} + 1\right)\frac{\sin x}{x} - \frac{5}{x^2}\left(\frac{21}{x^2} - 2\right)\cos x$
6	$\frac{1}{16}(231x^6 - 315x^4 + 105x^2 - 5)$	$\left(\frac{10\,395}{x^6} - \frac{4725}{x^4} + \frac{210}{x^2} - 1\right)\frac{\sin x}{x} - \frac{21}{x^2}\left(\frac{495}{x^4} - \frac{60}{x^2} + 1\right)\cos x$

The scattering from a distribution of independent molecules (or chain segments) is given by a convolution of the orientation distribution for the molecules with the scattering from a single molecule. If both the orientation distribution $D(\alpha)$ and the intramolecular scattering $i^m(s,\alpha)$ have cylindrical symmetry, then the resultant scattering $i(s,\alpha)$ also has cylindrical symmetry and all three functions can be expanded in Legendre series of even order. Moreover, Deas (1952) has shown that the coefficients of the three series are related by

$$i_{2n}(s) = \frac{2\pi}{4n+1} D_{2n} i^m_{2n}(s),$$

where $D(\alpha)$ is normalized such that

$$\int_0^{\pi/2} D(\alpha) \sin\alpha \, d\alpha = \frac{1}{2\pi}.$$

Hence, if i_{2n} and D_{2n} are known, we can derive the scattering from a single molecule (or chain segment).

Thus (2) becomes

$$i^m(s,\alpha) = \sum_{n=0}^{\infty} w_{2n} \, i_{2n}(s) P_{2n}(\cos\alpha)$$

where the extra weights, w_{2n}, are given by

$$\frac{1}{w_{2n}} = 2\pi \int_0^{\pi/2} D(\alpha) P_{2n}(\cos\alpha) \sin\alpha \, d\alpha = \langle P_{2n}(\cos\alpha)\rangle_D$$

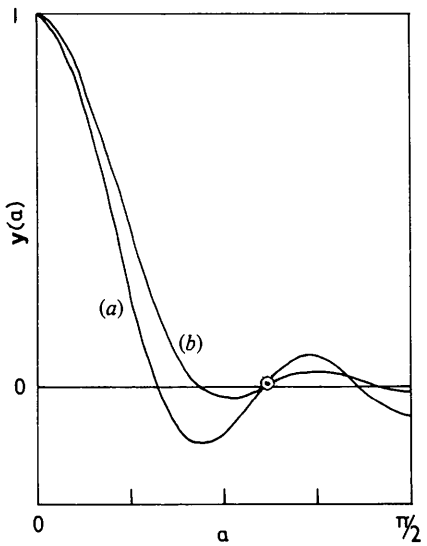

Fig. 2. The effect of truncation of the Legendre series for a meridional δ function. Truncation at four terms: (*a*) without window function

$$y = \frac{1}{4} \sum_{n=0}^{3} P_{2n}(\cos\alpha);$$

(*b*) with window function

$$y = \frac{2}{5} \sum_{n=0}^{3} \left(1 - \frac{n}{4}\right) P_{2n}(\cos\alpha).$$

and $\langle P_{2n}(\cos\alpha)\rangle_D$ are the orientation parameters of $D(\alpha)$ (Ward, 1977).

The form of $D(\alpha)$ can be derived from the halo with the sharpest azimuthal profile. A purely meridional halo such as the second or third haloes of PMMA gives $D(\alpha)$ directly, but with an equatorial halo such as for PS, the weighting factors must be calculated from

$$\frac{1}{w_{2n}} = \frac{\int_0^{\pi/2} I_{eq}(\alpha) P_{2n}(\cos\alpha) \sin\alpha \, d\alpha}{P_{2n}(0) \int_0^{\pi/2} I_{eq}(\alpha) \sin\alpha \, d\alpha}, \qquad (6)$$

where $P_{2n}(0) = (-1)^n[(2n)!/2^{2n}(n!)^2]$ (Lovell & Mitchell, 1981).

So far, our analysis has used infinite series, whereas the data only warrant a small number of terms. This truncation of the series leads to loss of resolution and, more importantly, can produce spurious features in the sharpened pattern. This is seen in curve (*a*) of Fig. 2 which shows the effect of truncating the series for a δ function at $\alpha = 0$. Multiplying the coefficients by a 'window function' can minimize the spurious features (curve *b* of Fig. 2). We have adopted a triangular window function of the form $(1 - n/N)$, where N is the number of terms used ($N = 4$ in our case). This is an arbitrary choice but it was found in practice to remove spurious features without increasing the loss of resolution.

Reduced intensity patterns sharpened by this method are presented later in this paper. Since the derivation of $D(\alpha)$ from the data makes no allowance for any intrinsic azimuthal width due to disorder (Pick, Lovell & Windle, 1980), the patterns are to some extent over-sharpened. However, the broadening caused by use of only a few terms of the series should counteract this.

Since, from (5), each term in the expansion of $i(s,\alpha)$ is independently related to each term in the expansion of $W(R',\alpha)$, the CDF calculated with the extra weights, w_{2n}, is sharpened by the same amount as $i^m(s,\alpha)$. We include such sharpened CDF's in the results that follow.

An alternative application of this analysis is to polymers with rigid chain segments (or to liquid crystals) for which the two-dimensional intramolecular scattering $i^m(s,\alpha)$ can be calculated from the known molecular conformation. The scattering due to the arrangement of the segments can then be derived from the experimental scattering and the s-dependent weights:

$$\frac{1}{w_{2n}(s)} = \int_0^{\pi/2} i^m(s,\alpha) \, P_{2n}(\cos\alpha) \sin\alpha \, d\alpha.$$

The scattering calculated could then be transformed to give a CDF for the segment axes.

For cylindrical coordinates, Vainshtein (1966) has calculated the axial projection of the CDF of molecular axes in a liquid crystal from the scattering along the equator (*i.e.* $\alpha = 90°$). Our method can, of course, give a complete CDF.

5. Calculating CDF's of model single chains

The atomic coordinates for a polymer chain are generated for a particular chemical configuration by specifying the bond lengths, bond angles and torsion angles. For a given polymer the bond angles and lengths may be considered constant and hence a local conformation of a chain can be defined by a set of torsion angles. We adopt the same convention for measuring bond angles and torsion angles as Lovell & Windle (1980).

Model CDF's are prepared by considering all pairs of atoms in the chain and sorting their interatomic vectors (weighted with the product of the number of electrons in each of the two atoms) into a two-dimensional histogram. This histogram contains sharp features since only fixed, point atoms are considered, together with perfect orientational order. To obtain peak widths comparable to those found in experimental CDF's, the model histograms are smeared, both radially and azimuthally in a similar manner to that described for RDF's (Waring, Lovell, Mitchell & Windle, 1981). Unlike the methods used for RDF's, an average density was not subtracted from the model CDF's and so they represent variations in the total electron density, rather than the differences as in the experimental reduced CDF's.

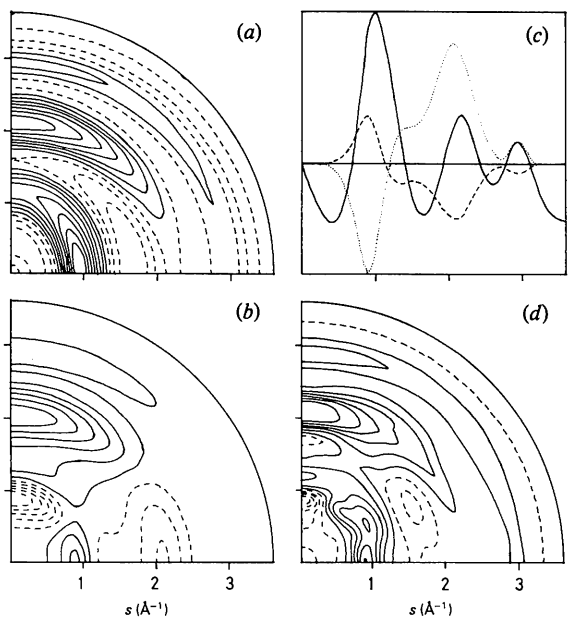

Fig. 3. Reduced intensity for atactic PMMA oriented by extrusion at 373 K. Dashed contours are negative. (*a*) Total intensity, $si(s,\alpha)$; (*b*) anisotropic component, $s[i(s,\alpha) - i_0(s)]$; (*c*) —— isotropic, $si_0(s)$, ... meridional section of anisotropic, – – – equatorial section of anisotropic; (*d*) sharpened pattern

$$s\sum_{n=0}^{3}\left(1-\frac{n}{4}\right)w_{2n}\,i_{2n}(s)\,P_{2n}(\cos\alpha).$$

6. Analysis of WAXS data

6.1. *Oriented PMMA*

Fig. 3(*a*) shows the reduced intensity for atactic PMMA which had been oriented by extrusion at 373 K to an extension ratio of ~3:1. The data are presented in the form $si(s,\alpha)$ which enhances the higher s region and shows the third halo more clearly. The anisotropic component of the reduced intensity is shown in Fig. 3(*b*). This is obtained by subtracting the isotropic component, $si_0(s)$ from $si(s,\alpha)$. Although the second and third haloes are purely meridional, the second halo shows a tendency to extend parallel to the equator rather than circumferentially. The first halo is mainly equatorial, although its elliptical shape shows there may be other components. Fig. 3(*c*) shows meridional and equatorial sections of the anisotropic scattering compared with the isotropic scattering. It can be seen that the second halo is the most distinctly anisotropic feature and we have previously used this halo to measure chain orientation in PMMA (Pick, Lovell & Windle, 1980). The anisotropic scattering decreases to

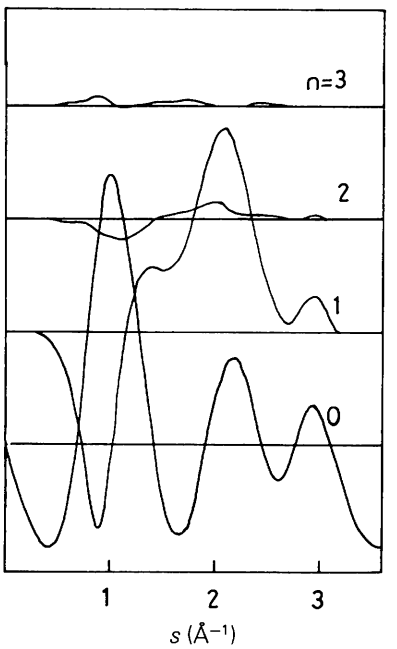

Fig. 4. Relative contributions of the different $i_{2n}(s)$ for PMMA.

zero by s_{max}, as required for minimum termination ripple in the CDF.

So far in the analysis, there has been no need to expand the anisotropic component in Legendre polynomials. This is, however, needed to obtain a sharpened scattering pattern. For the PMMA data, we found that only the first four terms ($n = 0$–3) were needed in (2) to represent $si(s,\alpha)$ within ~2% at all points. Fig. 4 shows the relative contributions of the different $i_{2n}(s)$.

The $i_2(s)$ term accounts for most of the anisotropic scattering. Since $P_4(\cos\alpha)$ is the first polynomial with an off-axis peak, this implies that all the features are predominantly meridional or equatorial. More terms in the expansion would have little effect on the CDF produced but would use slightly more computing time and, more importantly, give a greater probability of spurious features in the sharpened patterns since the weighting factors, w_{2n}, increase rapidly with n. Hence we have only used the first four terms in sharpening and transforming.

The azimuthally sharpened scattering pattern is shown in Fig. 3(*d*). We took the orientation distribution $D(\alpha)$ to be of the form $\cos^3\alpha$ which is a close approximation to the azimuthal profile of the third halo (the sharpest one). The most distinct features of the sharpened pattern are that the first halo apparently has two components: one on the equator and one at about 35° to the equator, and that the second and third haloes extend parallel to the equator.

The results of transforming the scattering are shown in Fig. 5. The inherent radial resolution in the transform is given by π/s_{max}, which is 0·87 Å for $s_{max} = 3{\cdot}6$ Å^{-1}. Nevertheless, the double peak at 7 and 9 Å, which is found in RDF's (Bjørnhaug, Ellefsen & Tønnesen, 1954; Mitchell & Windle, 1980), is well resolved in the total CDF (Fig. 5*a*). The main effect of orientation is to produce a broad equatorial peak near 8 Å which is more clearly seen in the anisotropic component of the CDF (Fig. 5*b*).

Meridional and equatorial sections of the anisotropic component are compared with the isotropic component (the RDF) in Fig. 5(*c*). It can be seen that the broad peak at ~15 Å is also equatorial. For convenience we have used straight lines to join the points given by the sampled transform. This, together with the small value of s_{max}, results in peaks which are more angular than would be expected from the reciprocal-space data.

Since the anisotropic component of the CDF must average to zero azimuthally, an equatorial trough gives rise to a meridional peak and *vice versa*. Hence we have only taken peaks to be real if they correspond to peaks in the isotropic component. The anisotropic component corresponds to the simplified CDF (Milberg, 1963) which suffers from these difficulties in interpretation.

The sharpened CDF is shown in Fig. 5(*d*). This demonstrates the equatorial nature of the 8 and 15 Å broad peaks more clearly. Also, the 7 and 9 Å peaks appear to be distinctly off-meridional.

The CDF's calculated for two model single chains of syndiotactic PMMA are shown in Fig. 6. Model (*a*) has the conformation proposed from analysis of the WAXS from unoriented PMMA (Lovell & Windle, 1980). A segment of chain in this conformation forms an arc and so the segment axis is taken as the tangent to the midpoint of the segment. Model (*b*) is a helix with

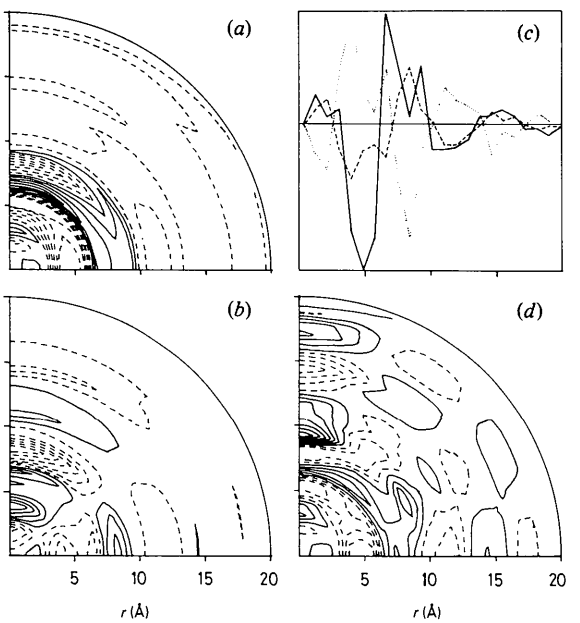

Fig. 5. Cylindrical distribution function for atactic PMMA. (*a*) Total CDF, $rW(r,\alpha)$; (*b*) anisotropic component

$$r\sum_{n=1}^{3} W_{2n}(r)\,P_{2n}(\cos\alpha);$$

(*c*) —— isotropic, $rW_0(r)$, ... meridional section of anisotropic, – – – equatorial section of anisotropic; (*d*) sharpened CDF

$$r\sum_{n=0}^{3}\left(1-\frac{n}{4}\right)w_{2n}\,W_{2n}(r)\,P_{2n}(\cos\alpha).$$

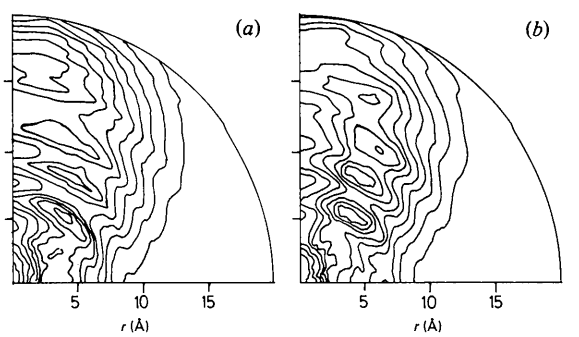

Fig. 6. CDF's for model single chains of syndiotactic PMMA (Lovell & Windle, 1980). (*a*) $(10°, 10°, -10°, -10°)_5$, $\theta_1 = 110°$, $\theta_2 = 128°$; (*b*) $(20°, 20°, 20°, 20°)_5$, $\theta_1 = 110°$, $\theta_2 = 128°$.

approximately 10 monomer units in one turn. It can be seen that both models are in quite good agreement with the sharpened experimental CDF.

6.2. *Oriented polystyrene*

The scattering from atactic PS oriented at 358 K is analysed in Fig. 7. Again there are three haloes. The first, though weak, is strongly equatorial whereas the second and third are predominantly meridional. However, as seen in Figs. 7(*b*) and (*c*), the anisotropic component only has a small feature corresponding to the third halo, the meridional intensification being mainly due to a long tail from the second halo. Sharpening, with the weights from (6), gives a pattern (Fig. 7*d*) similar to that produced by the iterative method (Lovell & Windle, 1976) and confirms our earlier findings that the second halo has an off-meridional component.

The meridional peaks beyond $s = 2{\cdot}0$ Å^{-1} appear to be a genuine feature which is most obvious in $i_6(s)$, although the magnitude of this component is close to the noise level of the data (Fig. 8).

The unsharpened CDF from PS (Fig. 9*a*) is surprisingly isotropic, showing the small effect that the highly oriented first halo has on the transform. The features in the CDF are mostly elliptical with distances slightly shorter parallel to the extension direction and slightly more of them. The intraphenyl distances are distinctly equatorial; this is particularly obvious in the anisotropic component (Fig. 9*b*).

The sharpened CDF (Fig. 9*d*) is distinctly different from the unsharpened one and gives peaks at distances near to those expected for the packing of phenyl groups. The interpretation of these CDF's is still in progress; however in Fig. 10 we show model CDF's for single chains in the two most likely conformations.

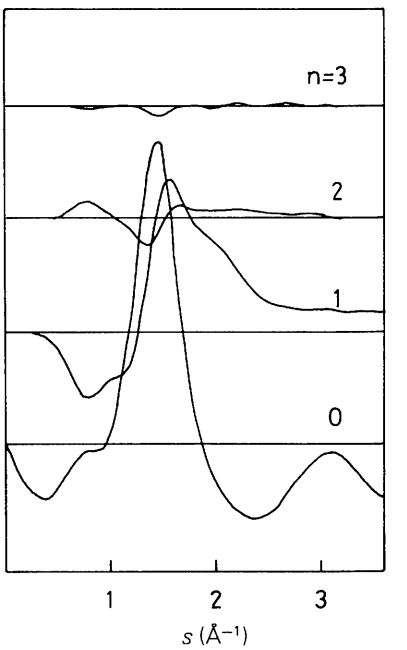

Fig. 8. Relative contributions of the different $i_{2n}(s)$ for PS.

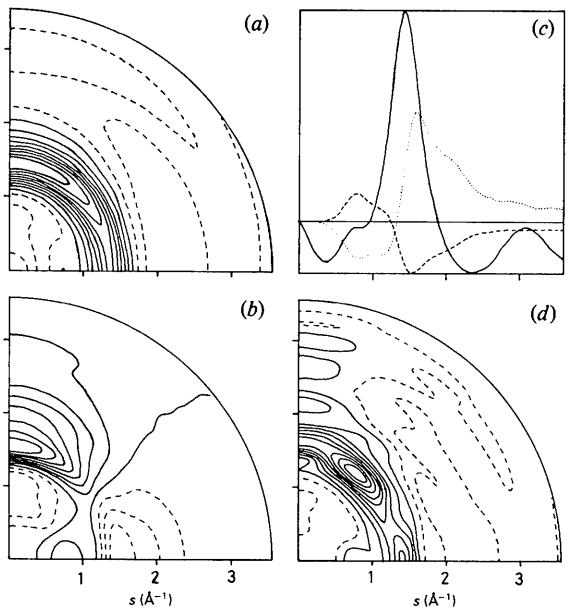

Fig. 7. Reduced intensity for atactic PS oriented by extrusion at 358 K. (*a*), (*b*), (*c*), (*d*): see Fig. 3.

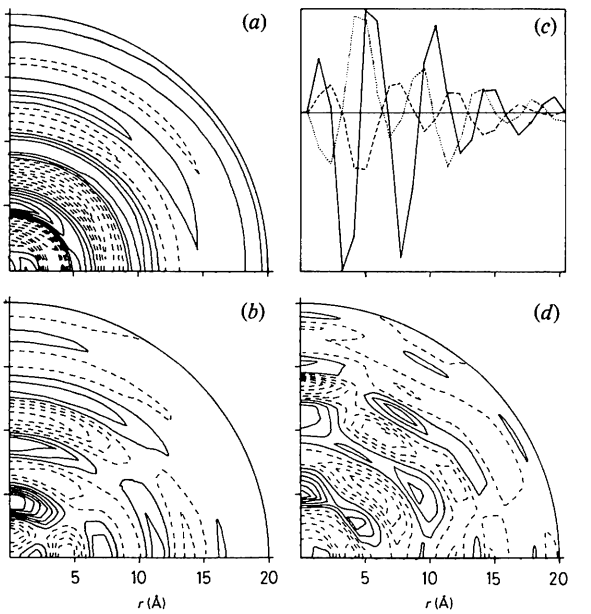

Fig. 9. CDF for atactic PS. (*a*), (*b*), (*c*), (*d*): see Fig. 5.

Model (*a*) is an all-*trans* planar zig-zag showing particularly good agreement with the experimental CDF. Model (*b*) is a helix with approximately four monomer units per turn and it is in much poorer agreement.

7. Conclusions

1. A systematic approach with spherical coordinates can produce reliable and useful CDF's for an oriented polymer.

2. Azimuthally sharpened scattering patterns and CDF's give more detail which can aid in the interpretation.

3. For atactic poly(methyl methacrylate), the 7 and 9 Å double peak in the RDF is shown to originate from intrachain distances but it is superimposed on a broader interchain peak at about 8 Å.

4. For atactic polystyrene, the packing of phenyl rings seems to correspond to that found in a syndiotactic planar zig-zag.

5. These techniques may also be applicable to the analysis of WAXS from liquid crystalline systems.

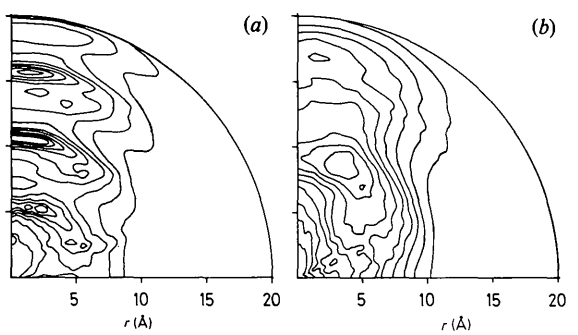

Fig. 10. CDF's for model single chains of syndiotactic PS. (*a*) $(tttt)_5$, $\theta_1 = 112°$, $\theta_2 = 114°$; (*b*) $(ttgg)_5$, $\theta_1 = 112°$, $\theta_2 = 114°$.

We acknowledge support and encouragement from Dr A. H. Windle during the course of this work, which was funded by the Science Research Council. The computer program for calculating spherical Bessel functions was supplied by Dr M. R. O'Donohue of the University of Cambridge Computing Service.

References

ABRAMOWITZ, M. & STEGUN, I. A. (1965). *Handbook of Mathematical Functions*, p. 452. New York: Dover.

ALEXANDER, L. E. (1969). *X-ray Diffraction Methods in Polymer Science*. New York: Wiley.

BJØRNHAUG, A., ELLEFSEN, Ø. & TØNNESEN, B. A. (1954). *J. Polym. Sci.* **12**, 621–632.

DEAS, H. D. (1952). *Acta Cryst.* **5**, 542–546.

DWIGGINS, C. W. (1972). *Acta Cryst.* A**28**, 155–159.

FILON, L. N. G. (1929). *Proc. R. Soc. Edinburgh*, **49**, 38–47.

KROGH-MOE, J. (1956). *Acta Cryst.* **9**, 951–953.

LOVELL, R. & MITCHELL, G. R. (1981). *Acta Cryst.* A**37**, 135–137.

LOVELL, R., MITCHELL, G. R. & WINDLE, A. H. (1979). *Acta Cryst.* A**35**, 598–603.

LOVELL, R., MITCHELL, G. R. & WINDLE, A. H. (1980). *Faraday Disc.* **68**, 46–57.

LOVELL, R. & WINDLE, A. H. (1976). *Polymer*, **17**, 488–494.

LOVELL, R. & WINDLE, A. H. (1977). *Acta Cryst.* A**33**, 390–395.

LOVELL, R. & WINDLE, A. H. (1980). *Polymer*. In the press.

MILBERG, M. E. (1963). *J. Appl. Phys.* **34**, 722–726.

MITCHELL, G. R. & WINDLE, A. H. (1980). *J. Appl. Cryst.* **13**, 135–140.

NORMAN, N. (1954). *Acta Cryst.* **7**, 462–463.

PICK, M., LOVELL, R. & WINDLE, A. H. (1980). *Polymer*, **21**, 1017–1024.

RULAND, W. (1977). *Colloid Polym. Sci.* **255**, 833–836.

VAINSHTEIN, B. K. (1966). *Diffraction of X-rays by Chain Molecules*, p. 253. Amsterdam: Elsevier.

WARD, I. M. (1977). *J. Polym. Sci. Polym. Symp.* **58**, 1–21.

WARING, J. R., LOVELL, R., MITCHELL, G. R., & WINDLE, A. H. (1981). To be submitted to *J. Mater. Sci.*

WARREN, B. E. (1969). *X-ray Diffraction*, p. 137. Reading, Mass.: Addison-Wesley.

WRINCH, D. (1946). *Fourier Transforms and Structure Factors*, p. 10, *Am. Soc. X-ray Electron Diffr. Monogr.* No. 2.